34th Annual International Conference of the IEEE EMBS
San Diego, California USA, 28 August - 1 September, 2012

Feasibility study of a trans-admittance mammography (TAM) system with 3600 current-sensing electrodes

Mingkang Zhao, Hun Wi, Abu Hena Mostofa Kamal,
Tong In Oh, *Member, IEEE,* and Eung Je Woo, *Senior Member, IEEE*

***Abstract*— We developed a trans-admittance mammography (TAM) system as a supplementary or alternative method of the X-ray mammography for screening and assessment of breast cancers. The breast is placed between a voltage applying electrode and 3600 current-sensing electrodes. Currents passing through the breast are measured by 72 current measurement channels on 12 ammeters cooperated with 6 switching modules. We sequentially measure exit currents 50 times with different switch configurations to make a projection image. Using planar electrode with 3600 current-sensing electrodes, we may improve the spatial resolution and distinguishability of projected images. We describe the design, construction and calibration of the first TAM system. We show TAM images of breast phantoms with known conductivity distributions at different frequencies.**

I. INTRODUCTION

Breast cancer is a multifactorial disease and the commonest cancer affecting women. Early detection of breast cancer through mammographic screening may reduce mortality [1]. Regular screening and assessment of breast cancer has been recommended to a postmenopausal woman who has a family history of that disease. Currently, it is extended to all women included premenopausal young women. X-ray mammography is the primary method to diagnose breast cancer among imaging techniques. The advantages and pitfalls of X-ray mammography have been examined by previous research works [2]. X-ray mammography uses ionizing radiation with a dose of 1 to 2.5 mGy per view. This ionizing radiation could be hazardous and induce malignancy. The risk of malignancy increases with the number of scans. And the sensitivity of X-ray mammography is reduced at a young age by dense breast tissue [3]. For this reason, there are several efforts to develop new methods to detect breast cancer such as a contrast enhanced MR imaging, scintimammography, confocal microwave imaging, and impedance imaging [4], [5], [6], [7], [8].

Impedance imaging may visualize a breast cancer since malignant breast tumors and normal tissues have significantly different electrical properties [9], [10], [11]. Kerner *et al* attached circular arrays of electrodes around the breast and produced cross-sectional conductivity images using the electrical impedance tomography (EIT) [12]. It did not provide enough spatial resolution and sensitivity to alter X-ray mammography. T-Scan was another approach for adjunctive clinical uses with X-ray mammography using a hand-held scan probe [13], [14]. It lacks a sophisticated reconstruction method of finding a lesion even though there were some clever works and observations in processing the trans-admittance data.

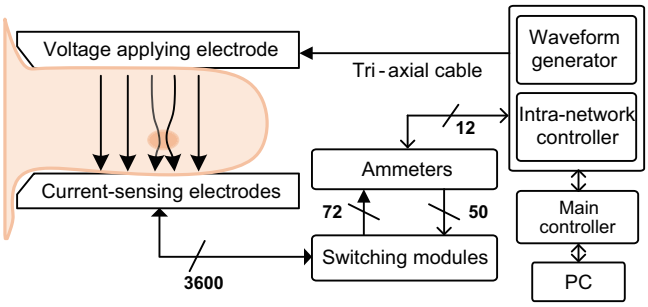

Fig. 1. Measurement configuration of the developed TAM system with 3600 current-sensing electrodes.

In this paper, we describe a new design of the trans-admittance mammography (TAM) system with better spatial resolution than conventional EIT. Because resolution of TAM is depended on the number of measurement electrodes and their distances. Instead of using the handheld voltage electrode and scan probe [13], [15], we use two plates with the breast between them. The imaging setup is identical to the X-ray mammography except the fact that we may rotate the two plates for consecutive projection imaging at any angle. The structure of TAM system is suitable to integrate with the X-ray mammography and recently developed anomaly detection algorithm can find the breast tumor without having to rely on the operator's skills [16]. We evaluate the performance of TAM system and produce trans-admittance images obtained at different frequencies.

II. METHODS

A. TAM structure

Figure 1 shows the measurement configuration and the structure of TAM system. Breast is placed between a voltage applying electrode and multiple current-sensing electrodes. We apply a constant voltage of 50 Hz to 500 kHz sinusoidal waveform to a large top plate. Amplitude of constant voltage source is controlled to maintain the amount of flowing current through the body below a safe range. On bottom plate is consisted of 3600 current-sensing electrodes kept at

Mingkang Zhao, Hun Wi, Abu Hena Mostofa Kamal and Eung Je Woo are with Impedance Imaging Research Center and the Department of Biomedical Engineering, College of Electronics and Information, Kyung Hee University, Yongin-si, Gyeonggi-do 446-701, Korea.

Tong In Oh is with Impedance Imaging Research Center and the Department of Biomedical Engineering, College of Electronics and Information, Kyung Hee University, Yongin-si, Gyeonggi-do 446-701, Korea (phone: 8231-201-3727; fax: 8231-201-2378; e-mail: tioh@khu.ac.kr).

the ground potential. From the potential difference between two plates, current spreads throughout the breast. It returns to the current-sensing electrode array. From this structure, we can get uniform current density distribution underneath the current-sensing electrodes when homogenous object case. A different conductivity anomaly inside the breast distorts the current flow and is mapped on the plane of current-sensing electrodes as a projected image. The measured exit current is varied by the trans-admittance distribution due to the configuration of normal and cancer tissues.

B. Switching module

Each current-sensing electrode is a gold-coated circular type with 2 mm radius produced by standard PCB technique. It has contact impedance of 14.8 $k\Omega$ at 50 Hz. The gap between adjacent electrodes in both x- and y-direction is 3 mm. On the back side of the electrode plate, we place 18 BGA-type SMD connectors. Each connecter has 200 pins and each pin is connected to one current-sensing electrode. In order to measure exit currents from all current-sensing electrodes, we use 6 switching modules and one switching module is response to 600 electrodes. One switching module is connected to independent 12 current measurement channels in 2 ammeters. Total 72 current measurement channels in 12 ammeters acquire exit currents from the corresponding current-sensing electrodes, simultaneously. We sequentially measure an exit current from 50 different switch configurations to make a projection image from 3600 electrodes. Electrode output is switched either to the circuit ground or to an input of chosen trans-resistance amplifier (OPA602, Texas Instruments, USA).

C. Ammeter

One ammeter consists of functional blocks as shown in figure 2. The controller implemented on an FPGA (EP3C10F256C8N, Altera, USA) generates 50 switching control signals to a switching module for changing switch configuration synchronized with data acquisition time. The exit current from a selected electrode is connected to the input of current measurement channel. The front-end of each current measurement channel is a trans-resistance amplifier that converts the exit current from a selected electrode to the amplified voltage signal. The current to voltage (I/V) converter provides a virtual ground to the input for measuring exit current [17]. We amplify the output of I/V converter using a variable gain voltage amplifier and filter out the noise signal. The dynamic input range of ammeter is from 10 nA to 100 uA. A high speed ADC quantizes the amplified and filtered signal for digital demodulation. We implemented the digital phase-sensitive demodulators inside a controller for each current measurement channel in order to process data in parallel. The demodulator outputs are transferred to a PC for presenting images. The acquisition speed of TAM is 56 ms when operating at 10 kHz. The acquisition time is varied depending on the period of applying signal.

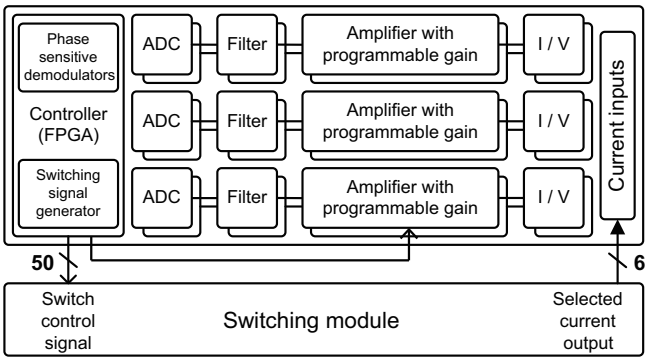

Fig. 2. The functional blocks of an ammeter included six current measurement channels.

D. Constant voltage source and controller

The intra-network controller and digital waveform generator are implemented on an FPGA. Intra-network controller arbitrates commands and data between the main controller (TMS320F2812, Texas Instruments, USA) and each ammeters through multiple serial ports in the star configuration. It is descended from the KHU Mark2 EIT system [18]. The constant voltage source consists of a latest DAC (AD9783, Analog Devices, USA) and operational amplifier. DAC component includes two 16-bit DACs for generating sinusoid waveform and two additional 10-bit DACs for compensating output offset and range controls. Analog outputs are summed to be fed to the power amplifier.

E. Calibration

Calibration is performed by using a rectangular saline tank whose top and bottom surfaces tightly fit the top and bottom plates of the TAM system. Inside the tank, we assume that current density is uniform and parallel to the z-direction. We choose one of measured exit current among the current-sensing electrodes at the center and find a complex scaling factor that makes a real number from the complex exit current. Using this real number as a reference value, we found 3599 complex scaling factors that make 3599 exit current values to be equal to the reference value. After obtaining the calibration table for the frequency of 500 Hz, we produced a calibration table of a chosen frequency comprising 3600 complex scaling factors that make all the exit current values at the frequency to be equal to the calibrated exit current values at 500 Hz.

III. Results

A. Performance of TAM system

Figure 3 shows the developed TAM system and 3600 gold-coated current-sensing electrodes placed underneath of testing object. The performance of TAM system was evaluated with crosstalk and signal-to-noise ratio (SNR) in figure 4. There are many current-sensing electrodes and switch configurations for measuring data with small number of measurement channels. We checked crosstalk between neighboring channels on the switches. The average crosstalk

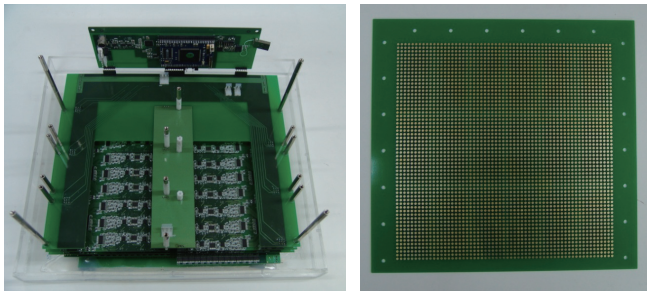

(a) (b)

Fig. 3. (a)TAM system and (b) 3600 channel gold-coated current-sensing electrodes.

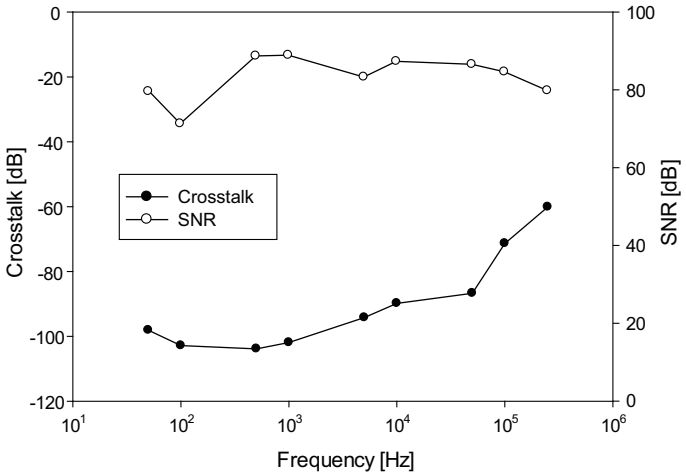

Fig. 4. Crosstalk between neighboring swtiches and SNR of TAM system

was -98.5 dB below 10 kHz. But it was varied up to -60 dB at 500 kHz.

We defined the SNR as the ratio of the mean value to the standard deviation of repeated measurements. Figure 4 shows SNRs from 50 Hz to 500 kHz using 100 repeated measurements for the magnitude of exit currents on the resistor phantom. The average SNR was 84.5 dB within the operating frequency range. It was degraded about 70 dB in the saline phantom. It was due to the thermal noise of electrodes.

B. Multi-frequency TAM imaging

We measured conductivity of background saline, agar, and carrot at the operating frequencies of the TAM system using an impedance analyzer (1260A, AMETEK Inc., UK). Figure 5 shows that the conductivity spectra of saline and agar had small variation than one of carrot. The conductivity spectrum of carrot was crossed over the conductivity spectrum of saline between 100 kHz and 250 kHz. The carrot has similar conductivity characteristic as biological tissues.

We prepared an agar object similar shaped as a trigonal prism with one side of 30 mm. The diameter of cylindrical carrot was 35 mm. Both objects have same height as 22 mm. We placed an agar object on the left side and a piece of carrot on the opposite side with same depth of 17mm. We

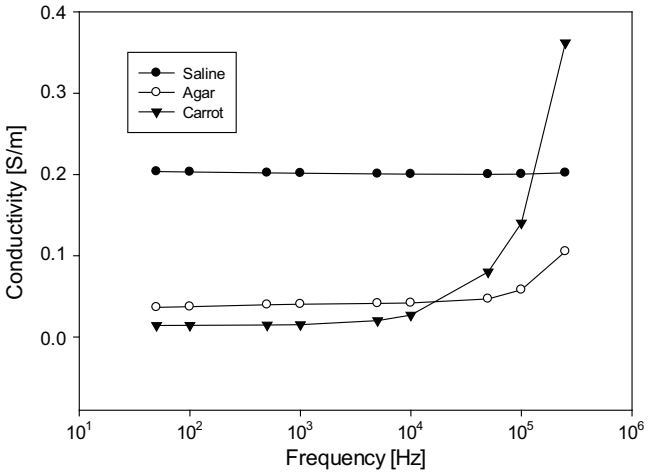

Fig. 5. Conductivity spectrum of background saline, agar, and carrot.

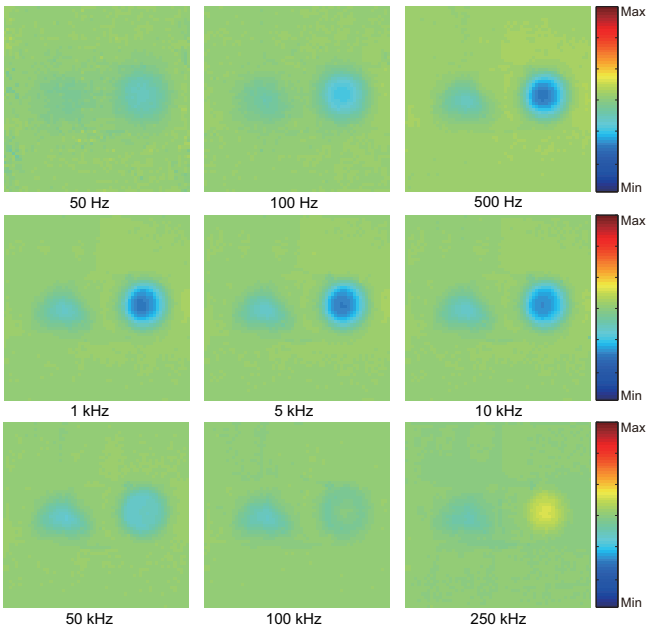

Fig. 6. Magnitude images of trans-admittance distribution obtained at 9 different frequencies.

displayed the relative conductivity map obtained at difference frequencies.

Figure 6 and 7 show the magnitude and phase images of trans-admittance distribution obtained at 9 different frequencies. The contrast of agar in the magnitude images didn't change over frequency range. The contrast change of carrot over the frequency range was matched as the variation of measured conductivity spectra for testing materials. Reconstucted conductivity contrast of carrot at 50 and 100 Hz had less than one of 500 Hz because signal was attenuated by the measurement system. In phase images, the phase for carrot was varied with operating frequency same as we expected.

IV. Discussion and Conclusion

We developed the TAM system produces trans-admittance projection images. We confirmed the performance of TAM

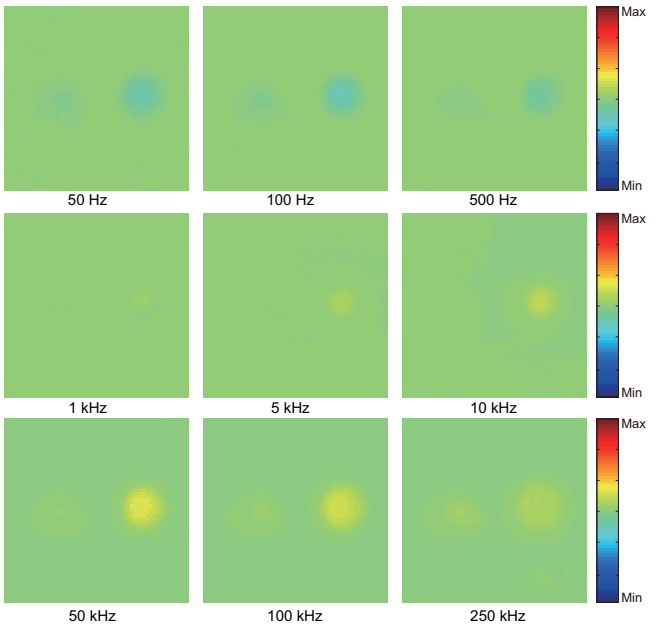

Fig. 7. Phase images of trans-admittance distribution obtained at 9 different frequencies.

system with crosstalk and SNR within operating frequency range. Even though crosstalk was increased by 40 dB at high frequency, SNRs were similar within frequency range. We produced the magnitude and phase images of trans-admittance distribution using a piece of carrot and agar in the saline phantom at 9 different frequencies. Contrast between background saline and anomalies were consistent with the conductivity spectra of testing materials. There is still problem for calibration at lower frequencies. However, we believe that the system is capable of detecting a small anomaly in the breast from trans-admittance projection images. The large number of current-sensing electrodes significantly improves their spatial resolution.

A TAM system is expected to be a supplementary or alternative method to detect the breast cancer. Mechanical structure of the system is similar to the X-ray mammography with the breast placed between two plates. The plates are movable to accommodate breasts with different sizes and rotatable to provide multiple images with different projection angles. We plan to incorporate a frequency-difference anomaly detection algorithm into the TAM system. For frequency analysis, the proper calibration method is required. We need to analyze relationship between the permittivity of anomaly and phase result. Also, we will integrate a TAM system with X-ray mammography to improve the assessment of detection for breast cancers. Finally, TAM system will be evaluated on animal and human models for clinical uses.

ACKNOWLEDGMENT

This work was supported by the National Research Foundation of Korea (NRF) grant funded by the Korea government (MEST) (No. 20100018275).

REFERENCES

[1] M. Reddy and R. Given-Wilson, Screening for breast cancer, Women's Health Medicine. 3, 1, pp. 22-27, 2006.
[2] S. A. Feig, Radiation risk from mammography: is it clinically significant?, AJR, 143, pp. 469-475, 1984.
[3] M. Popli, Physiology, pathology and imaging of the young breast, Indian J Radiol Imaging, 10, pp. 147-51, 2000.
[4] M. O. Leach, MARIBS study group, Screening with magnetic resonance imaging and mammography of a UK population at high familial risk of breast cancer: a prospective multicentre cohort study (MARIBS), 2005.
[5] J. B. Cwikla, J. R. Buscombe, S. M. Kelleher, S. P. Parbhoo, D. S. Thakrar, J. Hinton, A. R. Deery, J. Crow, A. J. W. Hilson, Comparison of accuracy of scintimammography and X-ray mammography in the diagnosis of primary breast cancer in patients selected for surgical biopsy, Clinical Radiology. 53, 4, pp. 274-280, 1988.
[6] A. E. Souvorov, A. E. Bulyshev, S. Y. Semenov, R. H. Svenson and G. P. Tatsis, Two-dimensional computer analysis of a microwave flat antenna array for breast cancer tomography, IEEE Trans. Microwave Theory Tech., 48, 8, pp. 1413-1415, 2000.
[7] Y. Zou and Z. Guo, A review of electrical impedance techniques for breast cancer detection Medical Engineering & Physics, 25, pp. 7990, 2003.
[8] A. Malich, T. Boehm, M. Facius, M. G. Freesmeyer, M. Fleck, R. Anderson and W. A. Kaiser, Differentiation of mammographically suspicious lesions: evaluation of breast ultrasound, MRI mammography and electrical impedance scanning as adjunctive technologies in breast cancer detection Clinical Radiology. 56, pp. 278-283, 2001.
[9] H. Fricke and S. Morse, The electrical capacity of tumors of the breast, J Cancer Res 10, pp. 340-376, 1926.
[10] J. E. Silva, J. P. Marques and J. Jossinet, Classification of breast tissue by electrical impedance spectroscopy, Med. Biol. Eng. Comput. 38, pp. 26-30, 2000.
[11] A. J.Surowiec, S. S. Stuchly, J. R. Barr and A. Swarup, Dielectric properties of breast carcinoma and the surrounding tissues, IEEE Trans. Biomed. Eng. 35, pp. 257-263, 1988
[12] T. E. Kerner, K. D. Paulsen, A. Hartov, S. K. Soho and S. P. Poplack, Electrical impedance spectroscopy of the breast: clinical imaging results in 26 subjects, IEEE Trans. Med. Imag. 21, pp. 638-645, 2002.
[13] M. Assenheimer, O. Laver-Moskovitz, D. Malonek, D. Manor, U. Nahliel, R. Nitzan and A. Saad, The T-Scan technology: electrical impedance as a disgnostic tool for breast cancer detection, Physiol. Meas. 22 pp. 1-8, 2001.
[14] B. Scholz, Towards virtual electrical breast biopsy: space-frequency MUSIC for trans-admittance data IEEE Trans. Med. Imag. 21, pp. 588-595, 2002
[15] T. I. Oh, J. H. Lee, J. K. Seo, S. W. Kim and E J Woo, Feasibility of breast cancer lesion detection using a multi-frequency trans-admittance scanner (TAS) with 10 Hz to 500 kHz bandwidth, Physiol. Meas. 28, S71-S84, 2007.
[16] S. Kim, Assessment of breast tumor size in electrical impedance scanning, Inverse Problems, 28, pp. 1-13, 2012.
[17] S. Franco, Design with Operational Amplifiers and Analog Integrated Circuits 3rd edn (New York: McGraw-Hill), 2002.
[18] T. I. Oh, H. Wi, D. Y. Kim, P. J. Yoo and E. J. Woo, Fully parallel multi-frequency EIT system with flexible electrode configuration: KHU Mark2, Physiol. Meas. 32, pp. 835-849, 2011.